

On the boundary condition for water at a hydrophobic, dense surface

By J. H. Walther[†], R. L. Jaffe[‡], T. Werder[†], T. Halicioglu[‡]
AND P. Koumoutsakos[¶]

We study the no-slip boundary conditions for water at a hydrophobic (graphite) surface using non-equilibrium molecular-dynamics simulations. For the planar Couette flow, we find a slip length of 64 nm at 1 bar and 300 K, decreasing with increasing system pressure to a value of 31 nm at 1000 bar. Changing the properties of the interface to from hydrophobic to strongly hydrophilic reduces the slip to 14 nm. Finally, we study the flow of water past an array of carbon nanotubes mounted in an inline configuration with a spacing of 16.4×16.4 nm. For tube diameters of 1.25 and 2.50 nm we find drag coefficients in good agreement with the macroscopic, Navier-Stokes values. For carbon nanotubes, the no-slip condition is valid to within the definition of the position of the interface.

1. Motivation and objectives

Macroscopic, Navier-Stokes modeling of problems in nano-fluidics may prove a computationally cost-effective alternative to themolecular-dynamics simulations usually employed at these length scales (Koplik & Banavar 1995) provided the complex fluid-solid interactions can find a suitable macroscopic model. At hydrophobic interfaces these interactions typically result in strong density fluctuations, anisotropic orientation of the water molecules (Lee *et al.* 1984), and, for solids with a high density, a finite fluid velocity (ΔU) at the interface (Helmholtz & von Piotrowski 1860; Schnell 1956; Churaev *et al.* 1984; Baudry *et al.* 2001). Thus while the kinematic boundary condition of impermeability follows naturally from the definition of a fluid-solid interface, the issues relating to momentum transfer at the interface determining the dynamics of the problem is less clear. At moderate shear rates ($\partial u / \partial y$) the fluid remains Newtonian (Loose & Hess 1989), and the slip velocity may be described by the linear relation:

$$\Delta U = L_s \frac{\partial u}{\partial y}, \quad (1.1)$$

where L_s is the slip length. Experimental evidence of slip has been demonstrated in studies of water in hydrophobized quartz capillaries (Churaev *et al.* 1984) and in drainage experiments (Baudry *et al.* 2001) with slip lengths of 30 ± 10 nm and 38 ± 2 nm, respectively. While most experiments have focused on the presence of slip at hydrophobic surfaces and on the possible validity of the no-slip condition at hydrophilic surfaces, recent colloid probe experiments with water on mica and glass have indicated a persistent slip of 8–9 nm at these hydrophilic surfaces (Bonaccorso *et al.* 2002). Molecular dynamics-simulations of Poiseuille flow (Barrat & Bocquet 1999; Travis *et al.* 1997; Travis & Gub-

[†] Institute of Computational Science, ETH Zürich, Switzerland

[‡] NASA Ames Research Center, USA

[¶] Institute of Computational Science, ETH Zürich, Switzerland and CTR/NASA Ames

1997; Cieplak *et al.* 2001) of simple Lennard-Jones fluids confined between Lennard-Jones solids have demonstrated the presence of both slip, no-slip and locking (negative slip length) depending on the “corrugation” of the surface. Thus, no-slip and locking are observed for low-density solids, and slip is found to occur at strongly non-wetting interfaces, or for high-density solids. In a recent study of methane confined between dense, graphite surfaces Sokhan *et al.* (2001) found the slip to be fairly insensitive to the wetting properties of the surface, but to depend strongly on the density of the solid.

In this paper we present detailed non-equilibrium molecular dynamics (NEMD) simulations of water confined between hydrophobic, dense (graphite) surfaces. For the planar Couette flow, we study the influence of the system pressure on the slip length, and on the wetting behaviour of the interface, by artificially increasing the carbon-water Lennard-Jones interaction. To study the effect of geometry on the slip, we consider simulations of water flowing past an array of carbon nanotubes. This flow configuration furthermore serves as a preliminary study of carbon nanotubes as sensing devices in aqueous environments.

2. Governing equations and solution procedure

The present study employs non-equilibrium molecular-dynamics (NEMD) simulations of water-graphite and carbon nanotube-water systems. In these simulations the graphite and the carbon nanotubes are treated as rigid structures, to permit the maximum time step of 2 fs imposed by the SPC/E water model. The influence of modelling the solids as rigid structures is expected to be minor, as demonstrated in the recent work of Sokhan *et al.* (2001). However, for the flow past carbon nanotubes, the deformation of the tubes imposed by the motion of the water may prove significant and will be included in later studies. The governing Newton’s equations are integrated in time using the leapfrog scheme, subject to periodic or quasi-periodic boundary conditions for the Couette and carbon nanotube flow problems, respectively. The algorithm has been parallelized using a domain decomposition technique and explicit message passing (MPI). The computational domain is distributed onto the processors and the atoms mapped accordingly. Atoms leaving their host processor during the simulation are sent to the receiving processor. The bond topology is described through global pointers, and mapped onto a local pointer set on the host processor. A decomposition onto 16 processors of the flow past a carbon nanotube is shown in figure 1. The simulations were performed on the SGI Origin 2000 cluster at NASA Ames.

2.1. Potentials

The water is modelled using the standard SPC/E model which involves a Lennard-Jones term between the oxygen atoms

$$U(r_{ij}) = 4\epsilon_{OO} \left[\left(\frac{\sigma_{OO}}{r_{ij}} \right)^{12} - \left(\frac{\sigma_{OO}}{r_{ij}} \right)^6 \right], \text{ for } r_{ij} < r_c, \quad (2.1)$$

where r_c is the radius of truncation ($U(r_{ij}) = 0$ for $r_{ij} > r_c$), and a Coulomb potential acting between all atom pairs from different water molecules

$$U(r_{ij}) = \frac{q_i q_j}{4\pi\epsilon_0 r_{ij}}, \quad (2.2)$$

where ϵ_0 is the permittivity in vacuum, and q_i is the partial charge, $q_O = -0.8476$ and $q_H = 0.4238$, respectively (Berendsen *et al.* 1987). The Coulomb interaction is computed

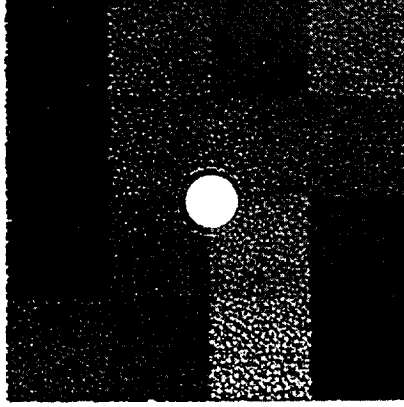


FIGURE 1. The parallel decomposition onto 16 processors for the NEMD simulations of the flow past a carbon nanotube. The different gray scale indicate the processor affiliation of the molecules.

using a smooth truncation as

$$U(r_{ij}) = \frac{q_i q_j}{4\pi\epsilon_0} \left(\frac{1}{r_{ij}} - E_s(r_{ij}) \right), \text{ for } r_{ij} < r_c, \quad (2.3)$$

where $E_s(r_{ij})$ is a smoothing function (Levitt *et al.* 1997)

$$E_s(r_{ij}) = \frac{1}{r_c} \left(1 - \frac{r_{ij} - r_c}{r_c} \right), \quad (2.4)$$

and $U(r_{ij}) = 0$ for $r_{ij} > r_c$. The truncation of the Coulomb potential has been shown to have little effect on the thermodynamic and structural properties of bulk water (Andrea *et al.* 1984), and for water at interfaces (Walther *et al.* 2001; Werder *et al.* 2002). In this study we employ a cutoff of 1.0 nm, throughout. The bond length (r_W) and bond angle (θ_W) of the water are constrained using SHAKE (van Gunsteren & Berendsen 1977).

The carbon-water interaction consists of a Lennard-Jones term between the carbon and oxygen atoms

$$U(r_{ij}) = 4\epsilon_{CO} \left[\left(\frac{\sigma_{CO}}{r_{ij}} \right)^{12} - \left(\frac{\sigma_{CO}}{r_{ij}} \right)^6 \right], \text{ for } r_{ij} < r_c, \quad (2.5)$$

and $U(r_{ij}) = 0$, for $r_{ij} > r_c$, and the parameters of the potential ϵ_{CO} and σ_{CO} are obtained from the experiments by Bojan & Steele (1987), with a modified ϵ_{CO} parameter obtained from molecular-dynamics simulations of the contact angle of water droplets on graphite (Werder *et al.* 2002). The parameters of the potentials are summarized in table 1.

3. Results

The results from the Couette and carbon nanotube studies are presented in terms of the time average profiles of the density

$$\rho_k = \frac{1}{V_k} \sum_i^{n_k} m_i, \quad (3.1)$$

$r_W = 1.000 \text{ \AA}$	$\theta_W = 109.47^\circ$	$\epsilon_{OO} = 0.6502 \text{ kJ mol}^{-1}$
$\sigma_{OO} = 3.166 \text{ \AA}$	$q_O = -0.8486 e$	$q_H = 0.4238 e$
$\epsilon_{CO} = 0.4389 \text{ kJ mol}^{-1}$	$\sigma_{CO} = 3.190 \text{ \AA}$	

TABLE 1. Parameters for the SPC/E water model (Berendsen *et al.* 1987), and for the carbon-water interaction potentials cf. (Bojan & Steele 1987) and (Werder *et al.* 2002). r_W , and θ_W denote the water bond length and angle, respectively, and q_O and q_H the partial charges. ϵ_{OO} and σ_{OO} are the SPC/E Lennard-Jones parameters, and ϵ_{CO} and σ_{CO} the carbon-water (oxygen) Lennard-Jones parameters.

and streaming velocity

$$\mathbf{v}_k = \frac{\sum_i^{n_k} m_i \mathbf{u}_i}{\sum_i^{n_k} m_i}, \quad (3.2)$$

where m_i and \mathbf{u}_i are the mass and velocity of the i -th atom, and n_k denotes the number of atoms in the k -th bin of volume V_k . The statistics for the Couette flow are sampled in Cartesian bins with a spacing in y -direction of 0.100 nm and 0.025 nm for the velocity and density profiles, respectively. A polar binning is used for the flow past a carbon nanotube with a radial bin resolution of 200 and 800 (a spacing of 0.32 and 0.08 nm) for the velocity and density profiles, respectively. The radial bins are subdivided in 6 bins in the circumferential direction. The slip length is extracted from the time average velocity profiles using a least square fit.

3.1. Couette flow

The simulations of the Couette flow involve from 240 to 1040 water molecules confined between a pair of (single) graphite sheets with a spacing of 1.35 nm to 4.72 nm depending on the system size and pressure. The size of the system in the streamwise (L_x) and spanwise (L_z) directions is 2.98×2.46 nm: see figure 2. The water molecules are initially placed on a regular lattice and the system is equilibrated for 40 ps to obtain a system temperature of 300 K and the desired pressure. Periodic boundary conditions are imposed in the streamwise and spanwise directions, and free space conditions are assumed in the wall-normal (y) direction. A Berendsen thermostat (Berendsen *et al.* 1984) is applied to adjust both the temperature and pressure, thus

$$L_y^{n+1} = L_y^n \left(1 - \frac{3\delta t}{\tau_p} (P_0 - P^n) \right), \quad (3.3)$$

where L_y^n denotes the spacing between the graphite sheets at the n -th time step, τ_p is the time constant of the thermostat (here $\tau_p = 0.1$ ps), and P_0 and P^n are the target and instantaneous pressure, respectively. The pressure is measured from the total normal forces acting on the graphite sheets as

$$P^n = \frac{1}{2L_x L_z} \sum_i^{n_c} \mathbf{f}_i^n \cdot \mathbf{n}_i, \quad (3.4)$$

where \mathbf{f}_i^n denotes the force acting on the i -th carbon atom, n_c is the total number of carbon atoms, and \mathbf{n}_i is the surface normal; see figure 2. The pressure bath is switched off after 40 ps, while maintaining the heat bath until 42 ps. The upper graphite wall is set into motion after 50 ps with a constant velocity (U) of 100 m s^{-1} throughout the 6 ns

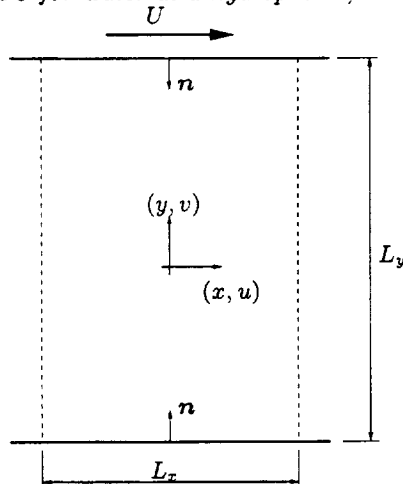


FIGURE 2. Sketch of the planar Couette flow problem. L_x and L_y denote the length of the unit cell in the streamwise (x) and wall-normal direction (y). The upper wall is forced to move with a constant velocity (U) and periodic boundary conditions are enforced in the streamwise and the spanwise (z) directions.

case	n_w	ϵ_{CO} kJ mol $^{-1}$	P (bar)	H (nm)	L_s (nm)
1	1040	ref.	10	4.72	63
2	1040	ref.	200	4.71	63
3	1040	ref.	500	4.60	42
4	1040	ref.	1000	4.50	31
5	1040	+50 %	200	4.66	33
6	1040	+100 %	200	4.59	14
7	800	ref.	200	3.70	41
8	240	ref.	200	1.35	∞

TABLE 2. Simulation cases for the planar Couette flow conducted at 300 K and pressures (P) of 10, 200, 500, and 1000 bar, respectively. The reference water-graphite van der Waals interaction given by ϵ_{CO} is 0.4389 kJ mol $^{-1}$ (Werder *et al.* 2002). H denotes the spacing between the graphite surfaces, and L_s the slip length. n_w is the number of water molecules, and 560 carbon atoms were used in all the cases.

of simulation. The system did not experience any appreciable viscous heating during the course of the simulation. The results are summarized in table 2.

We first consider the influence of the system pressure on the amount of slip for system pressures of 10, 200, 500, and 1000 bar using the reference carbon-water interaction potential. At these pressures the time-average profiles of the streaming velocity shown in figure 3 reveal a decreasing slip length for increasing pressure, resulting in a slip of 63, 63, 42, and 31 nm, respectively. The peaks in the profiles for $|x| > 2$ nm are caused by the poor sampling at the interfaces. The large fluctuations in the pressure typical of these small systems lead to similar results for the 10 and 200 bar system. The tendency for decreasing slip with increasing system pressure is in agreement with the recent NEMD simulations of Lennard-Jones fluids confined between Lennard-Jones solids by Barrat & Bocquet (1999). Moreover, the magnitude of the slip is in good agreement with the experimental values of 30–40 nm: see Churaev *et al.* (1984) and Baudry *et al.* (2001).

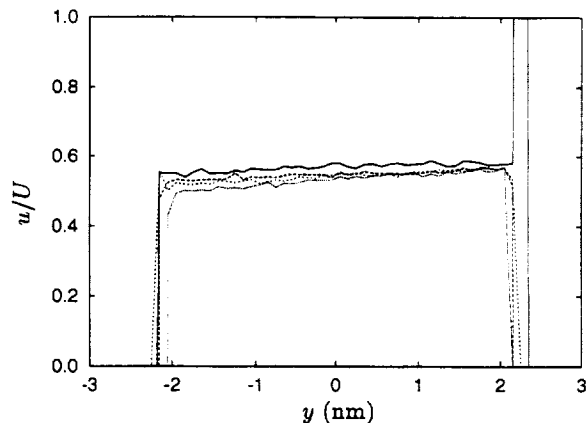


FIGURE 3. Time average streaming velocity profiles in a Couette flow as function of the system pressure: —: 10 bar (case 1); - - : 200 bar (case 2); - · - : 500 bar (case 4); · · · : 1000 bar (case 4).

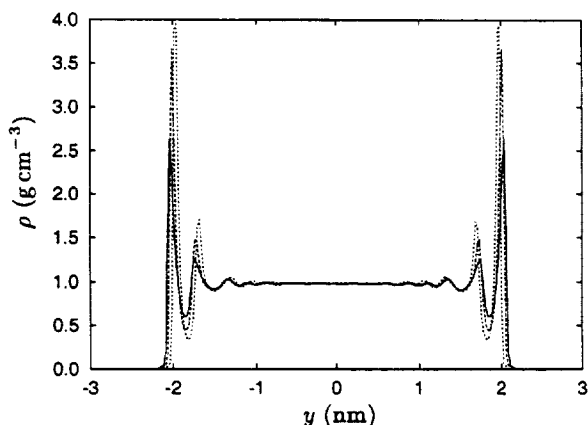


FIGURE 4. Time average density profile in a Couette flow as function of the wetting properties of the fluid-solid interface: —: $\epsilon_{CO} = 0.4389 \text{ kJ mol}^{-1}$ (case 2); - - : $\epsilon_{CO} = 0.6594 \text{ kJ mol}^{-1}$ (case 5); - · - : $\epsilon_{CO} = 0.8778 \text{ kJ mol}^{-1}$ (case 6).

Next we consider the influence of the wetting properties of the graphite-water interface by varying the strength of the Lennard-Jones interaction potential through an increase of the ϵ_{CO} parameter from the reference value of $0.4389 \text{ kJ mol}^{-1}$ by 50% ($0.6594 \text{ kJ mol}^{-1}$) and 100% ($0.8778 \text{ kJ mol}^{-1}$). The corresponding macroscopic contact angle for these interaction potentials for water droplets on graphite is 85° , 30° , and 0° , respectively (Werder *et al.* 2002). The time average density profiles shown in figure 4 display the characteristic fluctuations at a solid surface with increased peak values for increased wetting. The corresponding streaming velocity shown in figure 5 reveals a marked influence on the slip length. Thus, the slip decreases from 63 nm for the reference interaction potential to 33 and 12 nm for the 50% and 100% systems, the latter in good agreement with the experimental value of 8–9 nm for water at a hydrophilic surface (Bonaccorso *et al.* 2002).

Finally, we consider the influence of the size of the system by changing the distance between the graphite sheets from 4.71 to 3.70 and 1.35 nm. The density profiles shown in

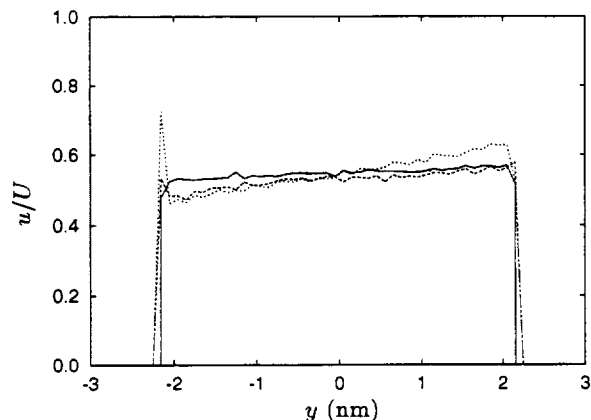


FIGURE 5. Time average streaming velocity profiles in a Couette flow as function of the wetting properties of the fluid-solid interface: —: $\epsilon_{CO} = 0.4389 \text{ kJ mol}^{-1}$ (case 2); - -: $\epsilon_{CO} = 0.6594 \text{ kJ mol}^{-1}$ (case 5); - · -: $\epsilon_{CO} = 0.8778 \text{ kJ mol}^{-1}$ (case 6).

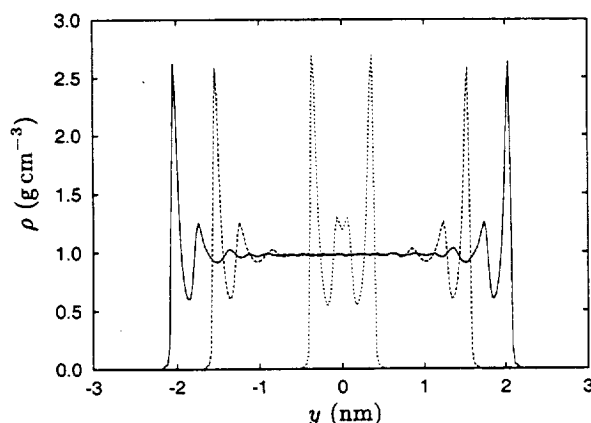


FIGURE 6. Time average density profile in a Couette flow as function of the size of the channel: —: $L_y = 4.71 \text{ nm}$ (case 2); - -: $L_y = 3.70 \text{ nm}$ (case 7); - · -: $L_y = 1.35 \text{ nm}$ (case 8).

figure 6 indicate the presence of bulk water at the center of the system for the 4.71 and 3.70 nm cases, whereas the density variations in the 1.35 nm case persist throughout the system. The velocity of the upper graphite sheet is 100 m s^{-1} for all systems, with an imposed shear of 2.0×10^{10} , 2.7×10^{10} and $7.4 \times 10^{10} \text{ s}^{-1}$, respectively, all below the critical value for water of approximately $12 \times 10^{10} \text{ s}^{-1}$ (Rahman & Stillinger 1971; Eisenberg & Kauzmann 1969). The results from the 3.70 nm system indicate a reduced slip length of 41 nm, and a very large slip for the 1.35 nm system. However, for the 1.35 nm system a longer sampling time appears to be required to determine the slip length with sufficient accuracy. The amount of thermal noise, and the presence of low-frequency oscillations in the system is demonstrated by the time history of the centerline velocity ($u(\frac{1}{2}L_y)$) as shown in figure 8. The centerline velocity is presented as a running mean with a time window of 40 ps for the 4.71 nm and 1.35 nm cases. The signals clearly contain low-frequency oscillations, with a period of approximately 0.5 ns, and similar to the fluctuations observed by Sokhan *et al.* (2001). Longer simulations including extended equilibration of

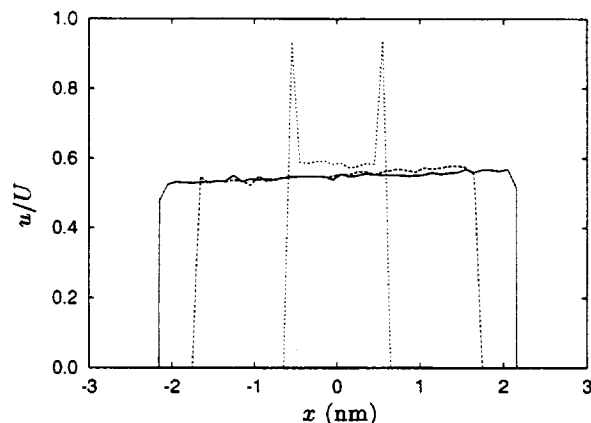


FIGURE 7. Time average streaming velocity profiles in a Couette flow as function of the size of the channel: —: $L_y = 4.71$ nm (case 2); - · -: $L_y = 3.70$ nm (case 7); · · ·: $L_y = 1.35$ nm (case 8).

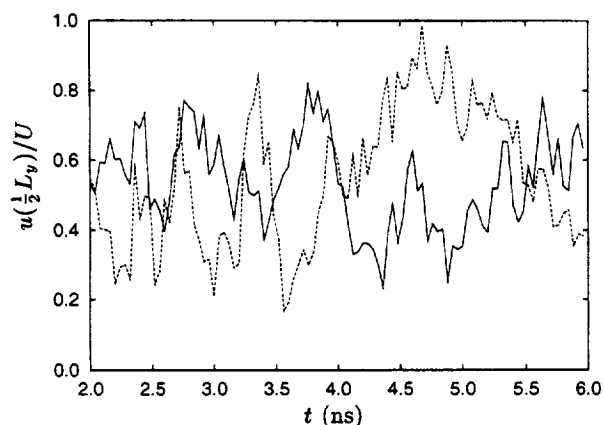


FIGURE 8. The time history of the running mean (40 ps averages) center line velocity in a Couette flow at different system sizes (L_y): —: 4.71 nm (case 2); - · -: 1.35 nm (case 8).

the system are currently being conducted to allow more accurate definition of the system pressure and of the slip length.

3.2. Flow past an array of carbon nanotubes

The flow past an array of carbon nanotubes is computed for tube diameters of 1.25 nm and 2.50 nm, to study the effect of curvature on the no-slip boundary condition and to compare the fluid forces acting on the array with macroscale Navier-Stokes models. The carbon nanotubes are (16,0) and (32,0) zigzag tubes, located at the center of the computational box with dimensions of $16.4 \times 16.4 \times 2.1$ nm. The total number of water molecules is approximately 18500, and the carbon nanotubes consist of 320 and 640 atoms for the 1.25 nm and 2.50 nm tubes, respectively.

The onset flow speed ($U = 50 \text{ m s}^{-1}$) is chosen sufficiently above the thermal noise to allow efficient sampling, but yet corresponding to a low Mach number ($\text{Ma} < 0.05$). During the first 4 ps of the 8 ps equilibration, the volume of the computational box is adjusted to match the target density of water (here $\rho = 0.997 \text{ g cm}^{-3}$) in the far-field, i.e.

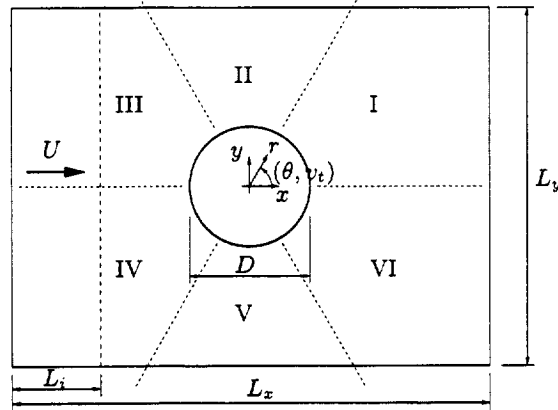


FIGURE 9. Sketch of the carbon nanotube-water system. D denotes the diameter of the carbon nanotube, L_x the size of the system in the streamwise direction, and L_y and L_x the height and width, respectively. The velocity of the center of mass of the water molecules contained in the “inlet” region (L_i) of the computational box is fixed to the desired value (U).

in the region defined by $r > R + \delta$, where $R = D/2$ is the tube radius, and $\delta = 0.8$ nm is chosen to exclude the region containing the density variations in the vicinity of the carbon nanotube (Walther *et al.* 2001). The regulation of the volume is performed by scaling the computational box in the x - y plane (see figure 9), while keeping the extent of the box in the z -direction fixed. The carbon nanotube is excluded from the scaling to preserve the radius of the tube. The flow is initially quiescent and impulsively turned on after 6 ps while maintaining the thermostat for the remaining 2 ps of the equilibration. The spatially-averaged streaming velocity is computed during the simulation and subtracted to allow equilibration of the peculiar velocities (i.e. the thermal component) only. The viscous heating during the 0.76 ns simulation was less than 8 K.

The flow speed is adjusted by monitoring the velocity of the center of mass of the water in the 3 nm (L_i) wide inlet region upstream of the carbon nanotube: see figure 9. In a leapfrog approximation, the velocity of the molecules is updated according to

$$\mathbf{v}^{n+1/2} = \mathbf{v}^{n-1/2} + \frac{\delta t}{m} (\mathbf{f} + \mathbf{b}), \quad (3.5)$$

where δt is the time step, m the mass of the molecule, and \mathbf{f} and \mathbf{b} denote the force and body force on the molecule, respectively. Thus, the center of mass velocity of the water molecules in the inlet region is updated accordingly

$$\mathbf{v}_{com}^{n+1/2} = \mathbf{v}_{com}^{n-1/2} + \frac{\delta t}{m_{tot}} (\mathbf{f}_{tot} + \mathbf{b}_{tot}), \quad (3.6)$$

where \mathbf{f}_{tot} is the total force acting on the center of mass of the molecules in the inlet region, and \mathbf{b}_{tot} is the total body force. In equation (3.6), \mathbf{b}_{tot} is adjusted to yield the desired center of mass velocity ($\mathbf{v}_{com}^{n+1/2} = \mathbf{U}$), thus

$$\mathbf{b}_{tot} = \frac{m_{tot}}{\delta t} (\mathbf{U} - \mathbf{v}_{com}^{n-1/2}) - \mathbf{f}_{tot}. \quad (3.7)$$

This boundary condition is equivalent to a prescribed total mass flow through the system and allows a non-uniform inlet velocity profile, and effectively modelling the flow past an array of carbon nanotubes arranged in an inline configuration.

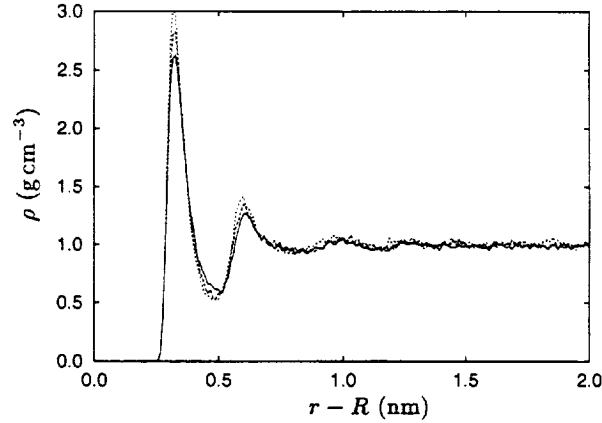


FIGURE 10. The time-average radial density profile for the flow past an array of 2.50 nm carbon nanotube. The profiles are sampled upstream, at the mid-section and downstream sections: —: section I; - - : section II; · · · : section III.

The simulations involve approximately 380000 time steps corresponding to 0.76 ns, with snapshots collected every 100 time steps (0.2 ps) starting at 0.4 ns for subsequent analysis. The time average density and streaming velocity profiles are sampled along the 6 radial bins as shown in figure 9. Both profiles exhibit symmetry across the x -axis, whereas asymmetries are discernable in the density profiles in the streamwise direction, in the vicinity of the carbon nanotube: see figure 10. The locations of the density extrema are similar for the three profiles, with the first peak located at $r - R = 0.32$ nm coinciding with the van der Waals equilibrium distance (σ_{CO}). However, the peak values decrease from 3.0 g cm^{-3} at the upstream direction (section III) to 2.8 g cm^{-3} and 2.6 g cm^{-3} for the sections II and I, respectively. Since the far-field density is constant with a value of approximately 1.0 g cm^{-3} , the observed asymmetry is ascribed to a local compression near the surface.

The amount of slip experienced in these systems is extracted from the tangential component (v_t) of the streaming velocity for the sections II and V shown in figure 11. The velocity profiles are similar but reach different free-stream values due to the different blockage ($(D - L_y)/L_y$) experienced by the flow. Since the Reynolds number (Re) based on the tube diameter and the fluid viscosity (ν) is less than unity, the velocity profile is fitted to the Stokes velocity field for a single circular cylinder (Batchelor 1967)

$$v_t = a \log\left(\frac{r}{R}\right) + b + c \frac{R^2}{r^2}, \quad (3.8)$$

where a , b , and c , are parameters of the fit. The fit is performed for the data shown in figure 11 in the interval $r \in [R + \sigma_{CO} : 7 \text{ nm}]$. We find, within the uncertainty of the fit and to within the accuracy of the definition of the location of the surface, that the no-slip condition is satisfied, i.e., $L_s < \sigma_{CO}$. We speculate that the difference between the amount of slip found in the planar Couette flow and in the flow past an array of carbon nanotubes is related to the amount of time the water is exposed to the solid surface ($\approx D/U = 25 - 50$ ps), and to the difference in the imposed external boundary conditions. Specifically, the driving mechanism of the Couette flow is the imposed shear, while for the Poiseuille flow (see e.g., Travis *et al.* (1997)) it is an imposed gravity (body) force. Since the present flow is driven by a body force imposed at the inlet section only,

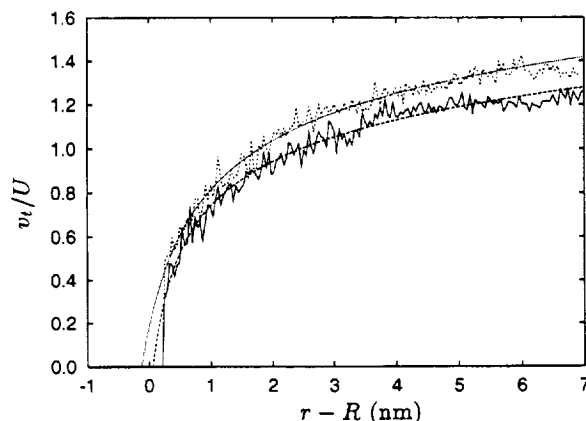


FIGURE 11. The time average tangential component of the streaming velocity for the flow past an array of carbon nanotubes. The profiles are sampled from section II and V and compared with equation (3.8) for the 1.25 nm tube: —: measured; - -: fit and the 2.50 nm tube: - · -: measured; · · ·: fit.

the remaining part of the flow is driven by a pressure gradient. To validate this conjecture we are currently performing simulations of Poiseuille flow driven by a pressure gradient, i.e. by imposing a body force in a limited inlet region similar to the present carbon nanotube study.

Finally, we consider the fluid forces (f_{β}) acting on the carbon nanotube array by computing the total force on the carbon atoms

$$f_{\beta} = \sum_i^{n_c} f_i. \quad (3.9)$$

The streamwise component of the force is compared with the Stokes-Oseen drag for the flow past an array of two-dimensional circular cylinders (Probstein 1994)

$$C_d = C_d^{cc} \frac{3 + 2\phi^{5/3}}{3 - \frac{9}{2}\phi^{1/3} + \frac{9}{2}\phi^{5/3} - 3\phi^2}, \quad (3.10)$$

where ϕ is the volume fraction (here $\phi = \pi R^2(L_x L_y)^{-1}$), and C_d^{cc} is the drag coefficient ($C_d = f_x(\frac{1}{2}\rho U^2 D)^{-1}$) on a single circular cylinder given by (Batchelor 1967)

$$C_d^{cc} = \frac{8\pi}{\text{Re} \log(7.4/\text{Re})}. \quad (3.11)$$

For the two cases $\phi_{1.25 \text{ nm}} = 0.0047$ and $\phi_{2.50 \text{ nm}} = 0.0183$, the Reynolds numbers are $\text{Re}_{1.25 \text{ nm}} = 0.063$, and $\text{Re}_{2.50 \text{ nm}} = 0.125$, resulting in drag coefficients (see equations 3.10 and 3.11) of 112 and 81 for the 1.25 nm and 2.50 nm tubes respectively. The measured forces are sampled from 0.40 ns to 0.66 ns using 13 samples of 20 ps each. The force components per unit length of the tube are $(126 \pm 19, 0 \pm 15, 0 \pm 4)$ kJ mol⁻¹ nm⁻¹ and $(159 \pm 19, 0 \pm 21, 0 \pm 5)$ kJ mol⁻¹ nm⁻¹, for the 1.25 nm and 2.50 nm tubes, respectively. The corresponding drag coefficients are 134 ± 20 and 85 ± 20 , both in good agreement with the Stokes-Oseen values. Thus, the hydrodynamic diameter of the carbon nanotube appears to be represented by the atomic center-to-center diameter of the carbon nanotube rather than an “effective diameter” based on the water density profile.

4. Summary and conclusions

We have presented non-equilibrium molecular dynamics simulations of water in a planar Couette flow and water flowing past an array of carbon nanotubes. For the planar Couette flow, we find a slip length of 63 nm at 300 K and 1 bar, decreasing to a value of 31 nm at higher pressures (1000 bar). By changing the properties of the interface from hydrophobic (contact angle of 85°) to hydrophilic (zero contact angle), the slip persists with a value of 14 nm. The values for both the hydrophobic and the hydrophilic interfaces are in good agreement with experimental values of 30–38 nm and 8–9 nm, respectively. Low frequency oscillations were observed in the velocity field and the simulations are currently being extended to secure a more accurate sampling.

Studies of the flow past an array of carbon nanotubes were also conducted to determine the effect of curvature on the amount of slip, and to compare the fluid forces with that of macroscopic Navier-Stokes models. For the two cases considered, with 1.25 nm and 2.50 nm zigzag carbon nanotubes mounted in an inline arrangement with a spacing of 16.4×16.4 nm, the no-slip condition appears to be valid. The extracted slip length is less than the van der Waals radius of the interface (< 0.3 nm). The hydrodynamic forces acting on the arrays are found to be in good agreement with macroscopic Navier-Stokes models, hence indicating that the integral fluid-dynamic properties of the system can be estimated using traditional fluid dynamics tools.

REFERENCES

- ANDREA, T. A., SWOPE, W. C. & ANDERSEN, H. C. 1984 The role of long ranged forces in determining the structure and properties of liquid water. *J. Chem. Phys.* **79**, 4576–4584.
- BARRAT, J.-L. & BOCQUET, L. 1999 Large slip effect at a nonwetting fluid-solid interface. *Phys. Rev. Lett.* **82**, 4671–4674.
- BATCHELOR, G. K. 1967 *An Introduction To Fluid Dynamics*, 1st edn. Cambridge University Press.
- BAUDRY, J., CHARLAIX, E., TONCK, A. & MAZUYER, D. 2001 Experimental evidence for a large slip effect at a nonwetting fluid-solid interface. *Langmuir* **17**, 5232–5236.
- BERENDSEN, H. J. C., GRIGERA, J. R. & STRAATSMA, T. P. 1987 The missing term in effective pair potentials. *J. Phys. Chem.* **91**, 6269–6271.
- BERENDSEN, H. J. C., POSTMA, J. P. M., VAN GUNSTEREN, W. F., DiNOLA, A. & HAAK, J. R. 1984 Molecular dynamics with coupling to an external bath. *J. Chem. Phys.* **81**, 3684–3684.
- BOJAN, M. J. & STEELE, W. A. 1987 Interactions of diatomic molecules with graphite. *Langmuir* **3**, 1123–1127.
- BONACCURSO, E., KAPPL, M. & BUTT, H.-J. 2002 Hydrodynamic force measurements: Boundary slip of water on hydrophilic surfaces and electrokinetic effects. *Phys. Rev. Lett.* **88**, 076103-1–076103-4.
- CHURAEV, N. V., SOBOLEV, V. D. & SOMOV, A. N. 1984 Slippage of liquids over lyophobic solid surfaces. *J. Coll. Interface Sci.* **97**, 574–581.
- CIEPLAK, M., KOPLIK, J. & BANAVAR, J. R. 2001 Boundary conditions at a fluid-solid interface. *Phys. Rev. Lett.* **86**, 803–806.
- EISENBERG, D. & KAUZMANN, W. 1969 *The Structure and Properties of Water*. Oxford University Press.

- VAN GUNSTEREN, W. F. & BERENDSEN, H. J. C. 1977 Algorithms for macromolecular dynamics and constraint dynamics. *Mol. Phys.* **37**, 1311–1327.
- HELMHOLTZ, H. & VON PIOTROWSKI, G. 1860 Über reibung tropfbarer flüssigkeiten. *Sitzungsberichte der Kaiserlich Akademie der Wissenschaften* **40**, 607–658.
- KOPLIK, J. & BANAVAR, J. R. 1995 Continuum deductions from molecular hydrodynamics. *Annu. Rev. Fluid Mech.* **27**, 257–292.
- LEE, C. Y., MCCAMMON, J. A. & ROSSKY, P. J. 1984 The structure of liquid water at an extended hydrophobic surface. *J. Chem. Phys.* **80** (9), 4448–4455.
- LEVITT, M., HIRSHBERG, M., LAIDIG, K. E. & DAGGETT, V. 1997 Calibration and testing of a water model for simulation of the molecular dynamics of proteins and nucleic acids in solution. *J. Phys. Chem. B* **101**, 5051–5061.
- LOOSE, W. & HESS, S. 1989 Rheology of dense model fluids via nonequilibrium molecular dynamics: shear thinning and ordering transition. *Rheol. Acta* **28**, 91–101.
- PROBSTEIN, R. F. 1994 *Physicochemical Hydrodynamics*. 2nd edition. Wiley, New York.
- RAHMAN, A. & STILLINGER, F. H. 1971 Molecular dynamics study of liquid water. *J. Chem. Phys.* **55**, 3336–3359.
- SCHNELL, E. 1956 Slippage of water over nonwetttable surfaces. *J. Appl. Phys.* **27**, 1149–1152.
- SOKHAN, V. P., NICHOLSON, D. & QUIRKE, N. 2001 Fluid flow in nanopores: An examination of hydrodynamic boundary conditions. *J. Chem. Phys.* **115**, 3878–3887.
- THOMPSON, P. A. & ROBBINS, M. O. 1990 Shear flow near solids: Epitaxial order and flow boundary conditions. *Phys. Rev. A* **41**, 6830–6841.
- THOMPSON, P. A. & TROIAN, S. M. 1997 A general boundary condition for liquid flow at solid surfaces. *Nature* **389**, 360–362.
- TRAVIS, K. P. & GUBBINS, K. E. 2000 Poiseuille flow of Lennard-Jones fluids in narrow slit pores. *J. Chem. Phys.* **112**, 1984–1994.
- TRAVIS, K. P., TODD, B. D. & EVANS, D. J. 1997 Departure from Navier-Stokes hydrodynamics in confined liquids. *Phys. Rev. E* **55**, 4288–4295.
- WALTHER, J. H., JAFFE, R., HALICIOGLU, T. & KOUMOUTSAKOS, P. 2001 Carbon nanotubes in water: Structural characteristics and energetics. *J. Phys. Chem. B* **105**, 9980–9987.
- WERDER, T., WALTHER, J. H., KOUMOUTSAKOS, P., JAFFE, R. L. & HALICIOGLU, T. 2002 On the water-graphite interaction for use in MD simulations. To appear in *J. Phys. Chem. B*.

